Journal of Hazardous Materials 189 (2011) 614–618

Contents lists available at ScienceDirect

Journal of Hazardous Materials

journal homepage: www.elsevier.com/locate/jhazmat

Short communication

Efficient degradation of tetrabromobisphenol A by heterostructured $Ag/Bi_5Nb_3O_{15}$ material under the simulated sunlight irradiation

Yingna Guo[a,b], Ling Chen[b], Fengyan Ma[b], Shengqu Zhang[b], Yuxin Yang[a], Xing Yuan[a,*], Yihang Guo[b,*]

[a] School of Urban and Environmental Sciences, Northeast Normal University, Changchun 130024, PR China
[b] School of Chemistry, Northeast Normal University, Changchun 130024, PR China

ARTICLE INFO

Article history:
Received 24 November 2010
Received in revised form 14 February 2011
Accepted 16 February 2011
Available online 23 February 2011

Keywords:
Bismuth niobate
Silver
Hydrothermal treatment
Photodeposition
Simulated sunlight photocatalysis
Brominated flame retardant

ABSTRACT

Heterostructured metallic silver-layered bismuth niobate two-component system ($Ag/Bi_5Nb_3O_{15}$) was developed for the first time by a mild hydrothermal method combined with photodeposition. The $Ag/Bi_5Nb_3O_{15}$ exhibited single-crystalline orthorhombic structure with small particle size (50–200 nm) and octahedral as well as sheet-like shape; additionally, it possessed photoresponse in both UV and visible region. As a novel alternative photocatalysts to TiO_2, the photocatalytic activity of the $Ag/Bi_5Nb_3O_{15}$ was evaluated by the degradation of tetrabromobisphenol A, a member from the family of the brominated flame retardant, under solar simulating Xe lamp irradiation, and enhanced photocatalytic activity in compared to $Bi_5Nb_3O_{15}$ itself and Degussa P25 was obtained.

1. Introduction

Photocatalysis has consistently drawn much attention for many of the environmental challenges facing the modern world since it can provide a simple way to use light to perform chemical transformation. Hazardous waste remediation, either in aqueous solutions or air, is the most extensively studied application of photocatalysis. Although TiO_2 has proven to be a promising candidate among various photocatalysts, its practical application is limited due to following two reasons: (i) quantum yield of TiO_2 is low owing to fast recombination of photoexcited hole (h^+) and electron (e^-); and (ii) TiO_2 has null photoresponse under visible light irradiation, which severely affects on the development of solar photocatalysis. Consequently, increasing research endeavors have been devoted to search for alternative photocatalysts to TiO_2 for detoxification of aqueous effluents with the assistance of the solar light. Among these, semiconductors based on cations with d^0 configuration such as Ta (V) [1], Nb (V) [2,3], or Ti (IV) [4], and oxides of d^{10} elements such as Bi (III) [1,2,4,5], In (III) [3,6], or Ga (III) [6,7] are among the most successful visible light-driven photocatalysts.

Our current work focuses on the development of metallic silver-layered bismuth niobate two-component heterostructure ($Ag/Bi_5Nb_3O_{15}$) as a novel and efficient photocatalyst. On the one hand, the valence band (VB) of $Bi_5Nb_3O_{15}$ is contributed by the hybridization of O2p orbit and Bi6s orbit, which leads to the elevated VB position of the compound and thereby the decreased band gap can be obtained. Accordingly, the photoresponse of $Bi_5Nb_3O_{15}$ is expected to extend to visible light region. On the other hand, deposition of silver particles throughout the interlayer space of the $Bi_5Nb_3O_{15}$ compound is expected to facilitate the separation of the photoexcited h^+ and e^- due to the strong electron accepting ability of metallic Ag particles; in addition, it is well known that noble metals (*e.g.* Au, Ag, and Pt) can strongly absorb visible-light due to the so-called surface plasmon resonance (SPR) effect; meanwhile, they also exhibit considerable UV-light response owing to the interband transition [8]. Therefore, Ag is a potentially photocatalyst that can utilize the full solar spectrum.

Conventionally, $Bi_5Nb_3O_{15}$ was synthesized by high temperature (*e.g.* 1100 °C) solid state reaction (SSR), which results in the compound with large crystal size (4–5 μm) [9]. Moreover, the photocatalytic performance of $Bi_5Nb_3O_{15}$ has seldom been studied expect for its ferroelectric and optoelectric properties. Herein, layered $Bi_5Nb_3O_{15}$ was successfully obtained by low temperature (200 °C) hydrothermal method; afterwards, metallic Ag particles were introduced into the interlayer space of $Bi_5Nb_3O_{15}$ by photochemical deposition. The photocatalytic activity of the resulting $Ag/Bi_5Nb_3O_{15}$ heterostructure was assessed by the degradation of a kind of light insensitive target compound, tetrabromobisphenol A (TBBPA), under simulated sunlight irradiation. TBBPA is the most widely used brominated flame retardant in the treatment of paper, textiles, plastics, electronic equipment and upholstered furniture. TBBPA is a nonvolatile and a non-mobile agent in soils

* Corresponding authors. Tel.: +86 431 85099561; fax: +86 431 85098705.
E-mail addresses: yuanx@nenu.edu.cn (X. Yuan), guoyh@nenu.edu.cn (Y. Guo).

0304-3894/$ – see front matter © 2011 Elsevier B.V. All rights reserved.
doi:10.1016/j.jhazmat.2011.02.054

and river sediments because of its limited water solubility, however, it is expected to leach out into ground waters and river at higher acidity. More recently, concerns have arisen due to the increasing occurrence of TBBPA in the environment and to the proven toxic and endocrine disruptor activity. TBBPA is difficult to be degraded under natural conditions, but it can be decomposed through anaerobic–aerobic biological process when microorganisms are domesticated for a long period [10]. Therefore, how to efficiently treat the wastewaters containing TBBPA is an important issue in the protection of ecosystems.

2. Experimental

2.1. Preparation of $Bi_5Nb_3O_{15}$

$Bi(NO_3)_3{\cdot}5H_2O$ (2 mmol) and $NbCl_5$ (1.4 mmol) was dissolved with ethanol (10 mL), respectively. With continuous stirring, the above $NbCl_5$ solution was slowly added to the $Bi(NO_3)_3$ solution. $NH_3{\cdot}H_2O$ was added into the mixture to adjust pH of 9, and then the solution was magnetically stirred for 0.5 h to obtain a white suspension. The white suspension was transferred into Teflon-lined stainless steel autoclave, and the autoclave was heated to 473 K for 24 h. After the reaction, the product was filtered and washed with distilled water and ethanol for three times, and then it was dried at 318 K for 12 h.

2.2. Preparation of $Ag/Bi_5Nb_3O_{15}$

$Bi_5Nb_3O_{15}$ powder (625 mg) was suspended in 90 mL $AgNO_3$ solution (0.10 mg/mL or 1.11 mg/mL). The resulting suspension was illuminated by an inserted high pressure mercury lamp (150 W) for 2 h under magnetic stirring. During illumination, the suspension changed from pale yellow to gray black. The gray black powder was recovered by centrifugation and then rinsed continuously with distilled water until no Ag^+ was detected in the eluate. Finally, the product was dried in an oven at 318 K for 12 h, and it is denoted as $Ag/Bi_5Nb_3O_{15}$-1 (Ag doping level of 1%) and $Ag/Bi_5Nb_3O_{15}$-10 (Ag doping level of 10%), respectively.

For comparison, $Pt/Bi_5Nb_3O_{15}$-1 (Pt doping level of 1%) was also prepared following the above route by using $H_2PtCl_6{\cdot}6H_2O$ (0.19 mg/mL) as a Pt source.

X-ray diffraction (XRD) patterns were obtained on a Japan Rigaku D/max 2000 X-ray diffractometer. Field emission scanning electron micrographs (FESEM) was obtained on a XL-30 ESEM FEG field emission scanning electron microscope at 20 kV. Transmission electron microscope (TEM) micrographs were recorded on a JEM-2100F high resolution transmission electron microscope at an accelerating voltage of 200 kV. X-ray photoelectron spectroscopy (XPS) was performed on a VG-ADES 400 instrument with Mg K-ADES source. UV–vis diffuse reflectance spectra (UV–vis/DRS) were recorded on a Cary 500 UV-Vis-NIR spectrometer. Nitrogen porosimetry measurement was performed on a Micromeritics ASAP 2020 M surface analyzer.

The photocatalytic degradation of TBBPA was conducted in a quartz reactor, as shown in Fig. S1 of Electronic Supporting Information. The diameter of the reactor is 63 mm, consistent with that of facula of the light resource. The light source (being placed *ca.* 15 cm above the reactor) was provided by a PLS-SXE300 Xe lamp (300 W, Beijing Trusttech Co. Ltd., China) equipped with an IR cut filter to remove most of IR irradiation (680–1100 nm). Consequently, the artificial solar light used here matches well with the natural solar light with main emission from 320 nm to 680 nm (see Fig. S2 of Electronic Supporting Information). The light intensity was adjusted to 150 mW cm^{-2} (1.5 AM) measured by a radiometer (OPHIR, Newport, USA). The suspension containing the solid catalyst (150 mg) and TBBPA (40 mg L^{-1}, 100 mL) solution was poured into the reactor. Due to the poor water solubility, a mixture of water/acetonitrile 50/50 (v/v) was employed to prepare TBBPA reaction solutions. The suspension was ultrasonicated for 10 min and then stirred in the dark for 120 min. Subsequently, the Xe lamp was turned on and the photocatalytic degradation reaction was conducted for the next 120 min. Changes of the concentrations of TBBPA in the reaction system were monitored by a Agilent 1200 high pressure liquid chromatography (HPLC): C_{18} column, UV detector (λ = 210 nm), and acetonitrile/water (80/20, v/v) was used as a mobile phase at a flow rate of 1.0 mL/min. Evolution of HPLC chromatograms during the adsorption and photocatalytic degradation of TBBPA in the above

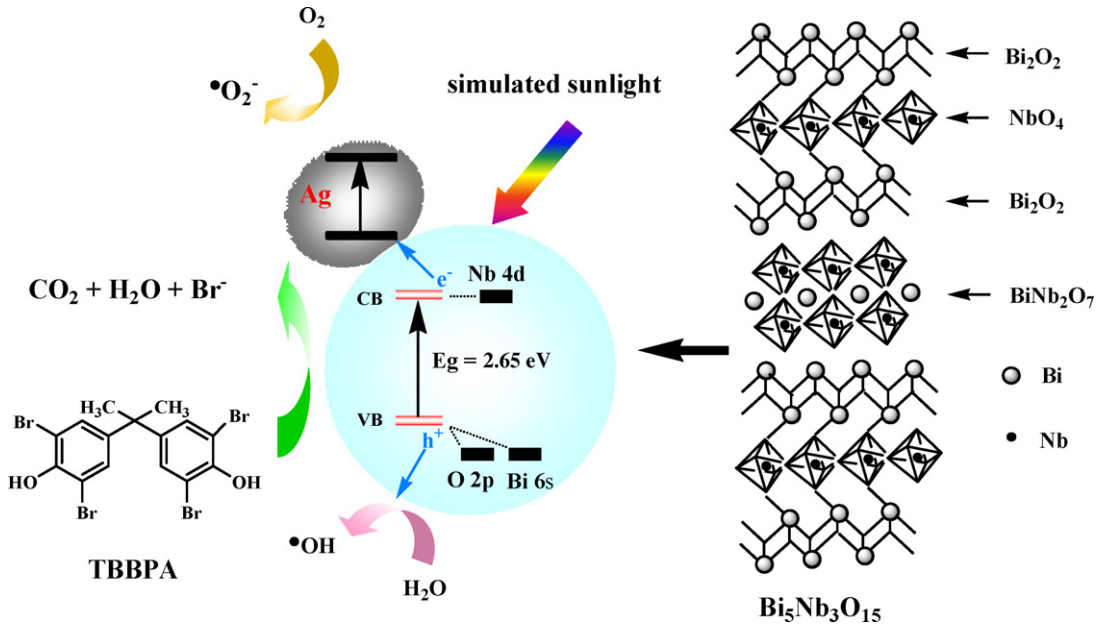

Scheme 1. The proposed band structure of $Ag/Bi_5Nb_3O_{15}$ as well as TBBPA degradation process over the simulated sunlight irradiated $Ag/Bi_5Nb_3O_{15}$.

system were provided in Fig. S3 of Electronic Supporting Information, and the peaks with the retention time of 5.9 min are originated from TBBPA. The concentration of Br^- ion (final product) was determined by a DX-300 ion chromatography (IC).

3. Results and discussion

It is reported that $Bi_5Nb_3O_{15}$ exhibits a mixed layered Aurivillius phase structure that can be expressed as $[Bi_2O_2]+[NbO_4]+[Bi_2O_2]+[BiNb_2O_7]$ (Scheme 1) [9]. Herein, the phase structure of as-prepared $Bi_5Nb_3O_{15}$ and $Ag/Bi_5Nb_3O_{15}$ samples was studied by XRD analysis (Fig. 1). As shown in Fig. 1, as-prepared $Bi_5Nb_3O_{15}$ compound exhibits a orthorhombic crystal structure with characteristic 2θ values of 29.22° (1 1 4), 32.60° (2 0 0), 33.88° (2 0 2), 46.82° (0 1 1 $\bar{0}$), 48.66° (2 2 1) and 57.79° (0 2 1 $\bar{0}$), respectively (JCPDS 16-0293). As for the $Ag/Bi_5Nb_3O_{15}$ heterostructure, its main diffraction peaks are still in accord with orthorhombic $Bi_5Nb_3O_{15}$; meanwhile, the cubic Ag phase can be observed with the characteristic 2θ value of 38.1° (1 1 1) (JPCDS 87-0720).

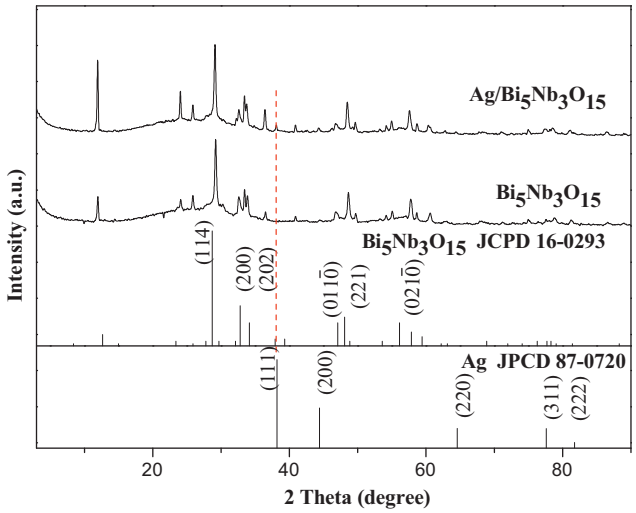

Fig. 1. XRD patterns of $Bi_5Nb_3O_{15}$ and $Ag/Bi_5Nb_3O_{15}$ samples.

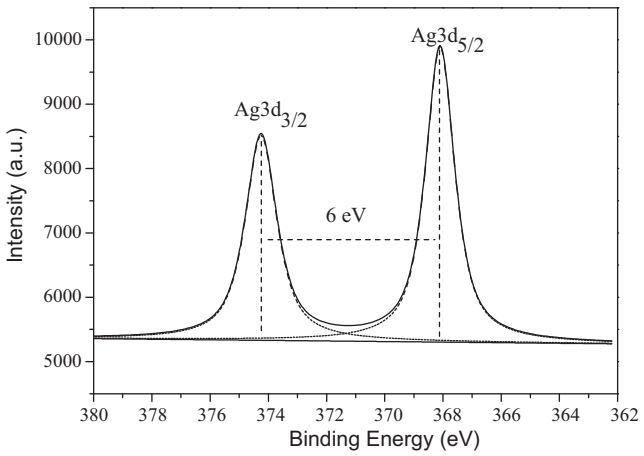

Fig. 2. High-resolution XPS spectrum of $Ag/Bi_5Nb_3O_{15}$ in the Ag3d binding energy region.

Doping metallic Ag throughout the layered $Bi_5Nb_3O_{15}$ compound is further confirmed by XPS surface probe technique (Fig. 2). The determined $Ag3d_{5/2}$ and $Ag3d_{3/2}$ binding energy of 368.2 eV and 374.2 eV and spin energy separation of 6.0 eV indicate that silver in the $Ag/Bi_5Nb_3O_{15}$ heterostructure is of metallic nature [11]. During the process of UV light illuminating $Bi_5Nb_3O_{15}$ in the presence of $AgNO_3$, the absorbed Ag^+ was reduced into metallic Ag^0 by the photoexcited electrons.

The morphology of $Bi_5Nb_3O_{15}$ and $Ag/Bi_5Nb_3O_{15}$ was revealed by FESEM and TEM technique (Fig. 3). Fig. 3a and b are the FESEM images of $Bi_5Nb_3O_{15}$ and $Ag/Bi_5Nb_3O_{15}$, respectively. From these

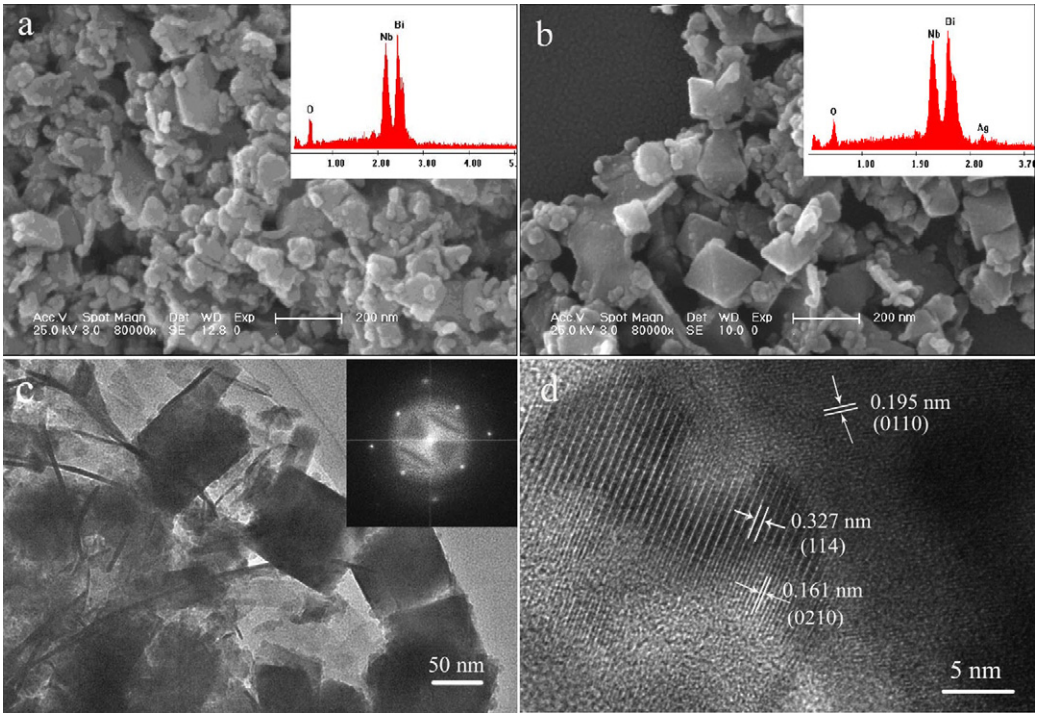

Fig. 3. FESEM images of (a) $Bi_5Nb_3O_{15}$ and (b) $Ag/Bi_5Nb_3O_{15}$; (c) TEM image of $Ag/Bi_5Nb_3O_{15}$; and (d) high-resolution TEM image of $Ag/Bi_5Nb_3O_{15}$. Inset of (a) and (b): EDX patterns of $Bi_5Nb_3O_{15}$ and $Ag/Bi_5Nb_3O_{15}$. Inset of (c): SAED pattern of $Ag/Bi_5Nb_3O_{15}$.

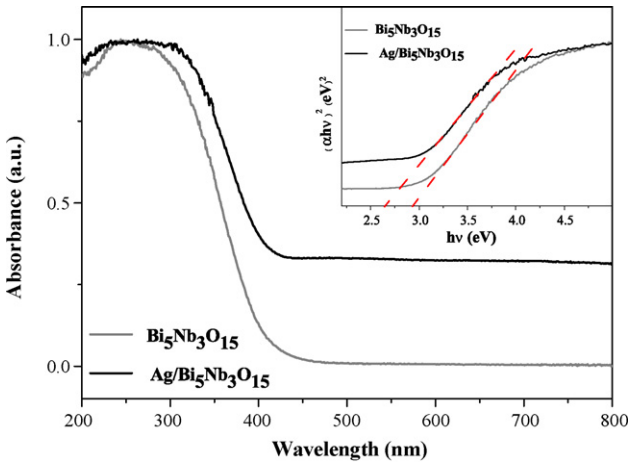

Fig. 4. UV–vis/DRS of $Bi_5Nb_3O_{15}$ and $Ag/Bi_5Nb_3O_{15}$ samples; inset is the plot of $(ah\nu)^2$ *vs* $h\nu$ for $Bi_5Nb_3O_{15}$ and $Ag/Bi_5Nb_3O_{15}$ samples.

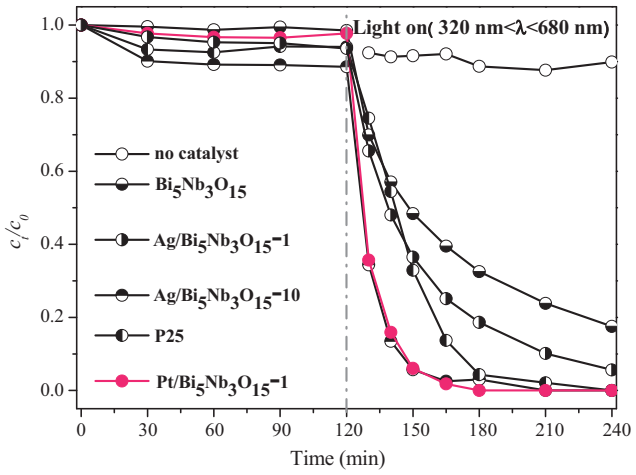

Fig. 5. Photodecomposition of TBBPA (c_0 = 40 mg/L, 100 mL) under simulated sunlight (320 nm < λ < 680 nm) irradiation over various photocatalysts (150 mg). c_0 and c_t refers to the concentration of TBBPA at initial and t time, respectively.

two images it is estimated that the particle size of $Bi_5Nb_3O_{15}$ and $Ag/Bi_5Nb_3O_{15}$ is in the range from 50 nm to 200 nm, and part of them show octahedral shape in addition to the sheet-like shape. The result demonstrates that the size and shape of $Bi_5Nb_3O_{15}$ remained intact after the deposition of Ag^0 clusters. Compared with SSR method, the particle size of $Bi_5Nb_3O_{15}$ obtained by hydrothermal reaction is smaller. EDX analysis result (insets of Fig. 3a and b) also indicates that Ag was successfully introduced into $Bi_5Nb_3O_{15}$ compound. The nanocrystalline nature of $Ag/Bi_5Nb_3O_{15}$ is visibly observed from the TEM images (Fig. 3c and d). The inset of Fig. 3c is the selected area electronic diffraction (SAED) of $Ag/Bi_5Nb_3O_{15}$, indicating single-crystalline orthorhombic $Ag/Bi_5Nb_3O_{15}$. The lattice fringe that is used for phase determination is 0.327 nm, 0.195 nm, and 0.161 nm observed in the high resolution TEM image, corresponding to the lattice spacings of (1 1 4), (0 1 1 $\bar{0}$), and (0 2 1 $\bar{0}$) plane of orthorhombic $Bi_5Nb_3O_{15}$, respectively (Fig. 3d).

Fig. 4 shows UV–vis diffuse reflectance spectra of $Bi_5Nb_3O_{15}$ and $Ag/Bi_5Nb_3O_{15}$ samples. The absorption of $Bi_5Nb_3O_{15}$ appears in the range of 200–450 nm, which is assigned to the charge transfer (CT) from the hybrid orbit of O2p and Bi6 s (VB) to Nb4d orbit (CB) [12,13]. After deposition of Ag throughout the $Ag/Bi_5Nb_3O_{15}$, the CT band of $Bi_5Nb_3O_{15}$ has somewhat redshift (with edge of *ca.* 500 nm) accompanying with a new absorption showed up in the range of 400–800 nm. Such absorption originates from the SPR effect of metallic Ag nanoparticles, further substantiating the formation of Ag^0 in as-prepared heterostructure [14]. For a crystalline semiconductor, the optical absorption near the band edge follows Kubelka–Munk formula $\alpha h\nu = A(h\nu - E_g)^{n/2}$, where α, ν, E_g and A are the absorption coefficient, the light frequency, the band gap and a constant, respectively [15]. The band gaps (E_g) of $Bi_5Nb_3O_{15}$ and $Ag/Bi_5Nb_3O_{15}$ are therefore estimated to be *ca.* 2.92 eV and 2.65 eV from the onsets of the absorption edges (inset of Fig. 4).

The simulated sunlight photocatalytic activity of as-prepared $Bi_5Nb_3O_{15}$ and $Ag/Bi_5Nb_3O_{15}$ samples was evaluated by the degradation of TBBPA (40 mg/L) in CH_3CN/H_2O (1/1, v/v) system. For comparison, Degussa P25 and as-prepared $Pt/Bi_5Nb_3O_{15}$-1 were also tested under the same conditions. From the result shown in Fig. 5 it is observed that after stirring the suspension of the catalyst and TBBPA CH_3CN/H_2O solution for 30 min in the dark, decrease of TBBPA concentration reaches to 1%, 6%, 2%, 11%, and 2% for the $Bi_5Nb_3O_{15}$, Degussa P25, $Ag/Bi_5Nb_3O_{15}$-1, $Ag/Bi_5Nb_3O_{15}$-10, and $Pt/Bi_5Nb_3O_{15}$-1, respectively; and TBBPA concentration remains unchangeable with further increasing the stirring time to 120 min. The result indicates that adsorption–desorption equilibrium between TBBPA molecules and the catalyst is established after 30 min stirring. Through analyzing the textural parameters of $Bi_5Nb_3O_{15}$ and $Ag/Bi_5Nb_3O_{15}$ ($Pt/Bi_5Nb_3O_{15}$) it is found that $Ag/Bi_5Nb_3O_{15}$ ($Pt/Bi_5Nb_3O_{15}$) with lower Ag (Pt) doping level (*e.g.* 1%) possesses almost the same BET surface area and pore volume as those of pure $Bi_5Nb_3O_{15}$ (42–44 $m^2\,g^{-1}$, Fig. S4 of Electronic Supporting Information). In the case of $Ag/Bi_5Nb_3O_{15}$ with higher Ag doping level (*e.g.* 10%), its BET surface area has somewhat decrease (31 $m^2\,g^{-1}$), which is due to the fact that part of the interlayer space of the $Bi_5Nb_3O_{15}$ was occupied by Ag particles. Therefore, we think that the adsorption capacity of TBBPA on the surface of $Ag/Bi_5Nb_3O_{15}$ is influenced by both the textural properties of $Ag/Bi_5Nb_3O_{15}$ and Ag particles deposited.

In the absence of any photocatalyst, decrease of the TBBPA concentration is negligible after simulated sunlight irradiation for 120 min. However, significant degradation of TBBPA is found in the presence of both simulated sunlight irradiation and photocatalyst, and conversion of TBBPA reached to 95%, 94%, 67%, 64% and 52%, respectively, after simulated sunlight irradiating $Ag/Bi_5Nb_3O_{15}$-10, $Pt/Bi_5Nb_3O_{15}$-1, Degussa P25, $Ag/Bi_5Nb_3O_{15}$-1, and $Bi_5Nb_3O_{15}$ for 30 min. To further test the photocatalytic activity of $Ag/Bi_5Nb_3O_{15}$, its mineralization ability was evaluated by monitoring the concentration changes of Br^- ion produced during simulating Xe lamp irradiation of $Ag/Bi_5Nb_3O_{15}$-10 and TBBPA (Fig. S5 of Electronic Supporting Information). It shows the concentration of Br^- ion reached to its maximum value rapidly after the light irradiation for 30 min. In addition, eight intermediate products including 4-(2-hydroxyisopropyl)-2,6-dibromophenol (detected by HPLC as well as LC/ESI-MS and yielded after losing two Br atoms from TBBPA) and bisphenol A (detected by matrix-assisted laser desorption/ionization time-of-flight (MALDI-TOF/TOF)mass spectrometer and yielded after losing four Br atoms from TBBPA) were identified during the course of the degradation of an aqueous TBBPA. These results implied that $Ag/Bi_5Nb_3O_{15}$ can not only degrade TBBPA but also mineralize it efficiently.

The above catalytic tests indicate that as-prepared $Ag/Bi_5Nb_3O_{15}$ heterostructured system possesses excellent simulated sunlight photocatalytic activity towards TBBPA degradation, and its photoactivity outperforms pure $Bi_5Nb_3O_{15}$ as well as Degussa P25 TiO_2. On the one hand, the layered $Bi_5Nb_3O_{15}$ structure created a more favorable environment for the diffusion and separation of the h^+–e^- pairs. Moreover, the electrons photogenerated on the surface of the $Bi_5Nb_3O_{15}$ compound may be trapped by metallic Ag particles because of lower Fermi level of Ag [16]. Therefore, the photoexcited h^+ and e^- can be separated effec-

tively. The above two factors may lead to the $Ag/Bi_5Nb_3O_{15}$ system with the increased quantum efficiency with respect to $Bi_5Nb_3O_{15}$ itself. On the other hand, $Ag/Bi_5Nb_3O_{15}$ shows photoresponse in both UV and visible light region, accordingly, $Bi_5Nb_3O_{15}$ and Ag are excited simultaneously under the simulated sunlight irradiation, which gives higher population of the photoexcited e^- and h^+ to participate in the photocatalytic reaction with respect to Ag-free $Bi_5Nb_3O_{15}$ system. Accordingly, more active species like $O_2^{\bullet-}$ and $^{\bullet}OH$ radicals that are responsible for the decomposition of TBBPA can be produced [16–18]. The enhanced photocatalytic activity of $Pt/Bi_5Nb_3O_{15}$ in comparison to pure $Bi_5Nb_3O_{15}$ further supports the above explanation.

Based on the above discussion, the proposed band structure of $Ag/Bi_5Nb_3O_{15}$ as well as TBBPA degradation process over the simulating Xe lamp irradiated $Ag/Bi_5Nb_3O_{15}$ is illustrated in Scheme 1.

4. Conclusions

Single-crystalline orthorhombic $Ag/Bi_5Nb_3O_{15}$ heterostructure was successfully prepared by mild hydrothermal method combined with photodeposition. The process is cheaper and more environmentally friendly with respect to the traditional high temperature solid state reaction. As-prepared $Ag/Bi_5Nb_3O_{15}$ exhibited significantly highly simulated sunlight photocatalytic activity towards TBBPA degradation, and its activity outperformed $Bi_5Nb_3O_{15}$ itself and Degussa P25 TiO_2. The excellent photocatalytic activity of $Ag/Bi_5Nb_3O_{15}$ could be attributed to the synergistic effect of the layered structure of $Bi_5Nb_3O_{15}$, photoresponse in both UV and visible light region of $Ag/Bi_5Nb_3O_{15}$, and the electron trapping ability of metallic Ag particles.

Acknowledgments

This work is supported by the Key Project of Chinese Ministry of Education (308008); the Fundamental Research Funds for the Central Universities (09QNTD004); Natural Science Fund Council of China (20873018; 50878041); the Program of Changjiang Scholars and Innovative Research Team in University; and the Jilin Environmental Protection Bureau (2008-25).

Appendix A. Supplementary data

Supplementary data associated with this article can be found, in the online version, at doi:10.1016/j.jhazmat.2011.02.054.

References

[1] G. Zhang, M. Li, S. Yu, S. Zhang, B. Huang, J. Yu, Synthesis of nanometer-size Bi_3TaO_7 and its visible-light photocatalytic activity for the degradation of a 4BS dye, J. Colloid Interface Sci. 345 (2010) 467–473.
[2] H.G. Kim, D.W. Hwang, J.S. Lee, An undoped, single-phase oxide photocatalyst working under visible light, J. Am. Chem. Soc. 126 (2004) 8912–8913.
[3] L. Zhang, I. Djerdj, M. Cao, M. Antonietti, M. Niederberger, Nonaqueous sol–gel synthesis of a nanocrystalline $InNbO_4$ visible-light photocatalyst, Adv. Mater. 19 (2007) 2083–2086.
[4] X. Zhu, J. Zhang, F. Chen, Hydrothermal synthesis of nanostructures $Bi_{12}TiO_{20}$ and their photocatalytic activity on acid orange 7 under visible light, Chemosphere 78 (2010) 1350–1355.
[5] Y. Guo, X. Yang, F. Ma, K. Li, L. Xu, X. Yuan, Y. Guo, Additive-free controllable fabrication of bismuth vanadates and their photocatalytic activity toward dye degradation, Appl. Surf. Sci. 256 (2010) 2215–2222.
[6] H. Dong, Z. Li, X. Xu, Z. Ding, L. Wu, X. Wang, X. Fu, Visible light-induced photocatalytic activity of delafossite $AgMO_2$ (M=Al, Ga, In) prepared via a hydrothermal method, Appl. Catal. B: Environ. 89 (2009) 551–556.
[7] M.D. Hernández-Alonso, F. Fresno, S. Suárez, J.M. Coronado, Development of alternative photocatalysts to TiO_2: Challenges and opportunities, Energ. Environ. Sci. 2 (2009) 1231–1257.
[8] X. Chen, Z. Zheng, X. Ke, E. Jaatinen, T. Xie, D. Wang, C. Guo, J. Zhao, H. Zhu, Supported silver nanoparticles as photocatalysts under ultraviolet and visible light irradiation, Green Chem. 12 (2010) 414–419.
[9] S. Tahara, A. Shimada, N. Kumada, Y. Sugahara, Characterization of $Bi_5Nb_3O_{15}$ by refinement of neutron diffraction pattern, acid treatment and reaction of the acid-treated product with n-alkylamines, J. Solid State Chem. 180 (2007) 2517–2524.
[10] W.V. James, E.F. Donna, J. Kristi, M.M. Haggblom, Anaerobic biotransformation of tetrabromobisphenol A, tetrachlorobisphenol A, and bisphenol A in estuarine sediments, Environ. Sci. Technol. 36 (2002) 696–701.
[11] E. Stathatos, P. Lianos, P. Falaras, A. Siokou, Photocatalytically deposited silver nanoparticles on mesoporous TiO_2 films, Langmuir 16 (2000) 2398–2400.
[12] L. Zhang, H. Fu, C. Zhang, Y. Zhu, Effects of Ta^{5+} substitution on the structure and photocatalytic behavior of the $Ca_2Nb_2O_7$ photocatalyst, J. Phys. Chem. C 112 (2008) 3126–3133.
[13] A. Kudo, K. Omori, H. Kato, A novel aqueous process for preparation of crystal form-controlled and highly crystalline $BiVO_4$ powder from layered vanadates at room temperature and its photocatalytic and photophysical properties, J. Am. Chem. Soc. 121 (1999) 11459–11467.
[14] T. Hirakawa, P.V. Kamat, Charge separation and catalytic activity of $Ag@TiO_2$ core-shell composite clusters under UV-irradiation, J. Am. Chem. Soc. 127 (2005) 3928–3934.
[15] L. Wang, W. Wang, M. Shang, S. Sun, W. Yin, J. Ren, J. Zhou, Visible light responsive bismuth niobate photocatalyst: enhanced contaminant degradation and hydrogen generation, J. Mater. Chem. 20 (2010) 8405–8410.
[16] F. Zhang, Y. Pi, J. Cui, Y. Yang, X. Zhang, N. Guan, Unexpected selective photocatalytic reduction of nitrite to nitrogen on silver-doped titanium dioxide, J. Phys. Chem. C 111 (2007) 3756–3761.
[17] C. He, Y. Yu, X. Hu, A. Larbot, Influence of silver doping on the photocatalytic activity of titania films, Appl. Surf. Sci. 200 (2002) 239–247.
[18] B. Xin, Z. Ren, H. Hu, X. Zhang, C. Dong, K. Shi, L. Jing, H. Fu, Photocatalytic activity and interfacial carrier transfer of $Ag–TiO_2$ nanoparticle films, Appl. Surf. Sci. 252 (2005) 2050–2055.